

aiWave: Volumetric Image Compression with 3-D Trained Affine Wavelet-like Transform

Dongmei Xue, Haichuan Ma, Li Li, *Member, IEEE*, Dong Liu, *Senior Member, IEEE*, Zhiwei Xiong, *Member, IEEE*

Abstract— Volumetric image compression has become an urgent task to effectively transmit and store images produced in biological research and clinical practice. At present, the most commonly used volumetric image compression methods are based on wavelet transform, such as JP3D. However, JP3D employs an ideal, separable, global, and fixed wavelet basis to convert input images from pixel domain to frequency domain, which seriously limits its performance. In this paper, we first design a 3-D trained wavelet-like transform to enable signal-dependent and non-separable transform. Then, an affine wavelet basis is introduced to capture the various local correlations in different regions of volumetric images. Furthermore, we embed the proposed wavelet-like transform to an end-to-end compression framework called aiWave to enable an adaptive compression scheme for various datasets. Last but not least, we introduce the weight sharing strategies of the affine wavelet-like transform according to the volumetric data characteristics in the axial direction to reduce the amount of parameters. The experimental results show that: 1) when cooperating our trained 3-D affine wavelet-like transform with a simple factorized entropy module, aiWave performs better than JP3D and is comparable in terms of encoding and decoding complexities; 2) when adding a context module to further remove signal redundancy, aiWave can achieve a much better performance than HEVC.

Index Terms— Volumetric image compression, wavelet-like transform, lifting scheme, convolutional neural network, end-to-end image compression

I. INTRODUCTION

VOLUMETRIC images, including biological and medical images, are widely utilized nowadays due to the advance of imaging technology. Among all kinds of volumetric images, the biological images are mainly obtained by electron microscopy (EM) and play an essential role in investigating morphology and pathology of tissue cell. The medical images such as computer tomography (CT) and magnetic resonance imaging (MRI) have been applied to clinical diagnosis in most modern hospitals. However, the huge size of volumetric images brings huge challenges to hardware storage and transmission. For example, the raw brain images of drosophila occupy approximately 106 terabytes (TBs) of storage space [1]. To

Date of current version March 14, 2022. D. Xue, H. Ma, L. Li, D. Liu, and Z. Xiong are with the CAS Key Laboratory of Technology in Geo-Spatial Information Processing and Application System, University of Science and Technology of China, Hefei 230027, China (e-mail: xdm1@mail.ustc.edu.cn; hcma@mail.ustc.edu.cn; li1@ustc.edu.cn; dongeliu@ustc.edu.cn; zwxiong@ustc.edu.cn). Dr. Li Li is the corresponding author.

this end, exploring effective volumetric image compression techniques has become an urgent task.

In recent years, many methods have been proposed to address this challenge [2]–[7]. They can be roughly divided into three groups: video-based methods, autoencoder-based methods, and wavelet-based methods. Video-based methods, such as High Efficiency Video Coding (HEVC), are designed for natural videos. They treat one of the three spatial dimensions of volumetric images as temporal dimension and then estimate a motion field to exploit correlations in that dimension. However, in essence, the three spatial dimensions of volumetric images are the same and should be treated equally. Treating one spatial dimension as temporal dimension may limit the performance of video-based methods.

Thanks to the vigorous development of deep learning, autoencoder-based methods have developed rapidly and achieved the state-of-the-art image compression performance especially under low bitrate scenarios. However, autoencoder-based methods employ an irreversible transform module, which leads to uncontrollable losses when converting images into latent features. Therefore, they have been shown to have poor performance in the high bitrate scenarios [8]. Unfortunately, high-quality reconstruction is often needed to avoid fatal mistakes in volumetric image compression, and some application scenarios even require lossless reconstruction [9], [10]. To this end, the autoencoder-based compression methods are rarely used in volumetric image compression.

The most commonly used methods for volumetric image compression are based on wavelet. One representative method is JP3D [11], which is a 3-D extension of JPEG-2000 and has been widely used as a standard for volumetric image compression. The traditional wavelet used in JP3D can be implemented by constructing a wavelet basis or decomposing it into basic building blocks, e.g., lifting scheme. Through traditional wavelet, an input image can be converted from the pixel domain to a more energy-concentrated frequency domain. However, there are still many problems in JP3D, which seriously limits its performance. Firstly, the traditional wavelet basis in JP3D is designed manually with certain assumptions of the signal, e.g. smooth. But volumetric images are usually not ideal and follow those assumptions. Secondly, the traditional wavelet basis operates 1-D filters in three directions respectively thereby ignoring non-directional correlations. Thirdly, the traditional wavelet basis fails to handle various local contexts due to the fact that it shares wavelet basis functions in different positions of the entire image. Last

but not least, the traditional wavelet basis employed in JP3D is fixed and cannot be optimized according to specific data.

Motivated by the success of trained 2-D wavelets [12], [13], we propose a trained 3-D affine wavelet-like transform based on a lifting scheme to overcome the disadvantages of the traditional 3-D wavelet in JP3D. We replace the prediction and update filters in a lifting scheme with 3-D convolutional neural networks (CNNs). In this way, our trained 3-D affine wavelet is signal-dependent and can adapt to non-ideal signals. In addition, 3-D CNNs make it possible to capture correlations in any direction in 3-D space and can overcome the problems of traditional wavelet basis with only 1-D filters. Besides, compared with using the same wavelet basis globally in traditional wavelet, we introduce the affine wavelet-like transform to adaptively adjust the wavelet basis according to the local content. Moreover, we embed the proposed wavelet-like transform into a versatile end-to-end compression framework called aiWave. Last but not least, we introduce the weight sharing strategies of the affine wavelet-like transform according to the volumetric data characteristics in the axial direction to reduce the encoding and decoding complexities. Inheriting the advantages of wavelet transform, our affine wavelet-like transform is reversible and can meet the demand for high reconstruction quality of volumetric images.

Our main contributions are summarized as follows.

- We propose a versatile end-to-end compression framework called aiWave, which is composed of trained 3-D affine wavelet-like forward and inverse transforms, probability, and optional quantization and post-processing modules. It can be utilized for both lossy and lossless volumetric image compression.
- For the first time the affine wavelet-like transform is proposed and used for image compression. It is an adaptive and learnable wavelet-like transform that overcomes several shortcomings of traditional wavelet transform.
- Different weight sharing strategies are explored according to data characteristics to reduce the amount of parameters.

Part of this work has been published in our previous work [14]. In this paper, we further propose affine wavelet-like transform by utilizing adaptive wavelet basis to further overcome the shortcomings of traditional wavelet. In order to reduce the complexity of encoding and decoding processes, the weight sharing strategies is explored under different data characteristics. In addition, we propose aiWave-heavy by equipping our affine wavelet-like transform module with a more complex probability module, which finally improves the BD-PSNR by 2.312dB compared with our previous work. Furthermore, the medical image datasets are used to further explore the generalization performance of aiWave in 3-D images.

This paper is organized as follows. Section II introduces the related work. Section III describes the details of our aiWave framework. Section IV presents our experimental results and analysis. Section V concludes the entire paper.

II. RELATED WORK

In this section, we give an introduction to the existing methods for volumetric image compression. They can be

roughly divided into three groups: wavelet-based methods, video-based methods, and autoencoder-based methods.

A. Wavelet Transform and Its Variants

1) *Wavelet transform* : Wavelet transform is highly praised for its excellent decomposition ability. It can support both lossy and lossless compression. These advantages make it widely used in the field of volumetric image compression [15]–[17]. The representative methods based on wavelet transform is JP3D. It is the tenth part of JPEG-2000, an extension for 3-D images. Until now, it is the most widely used method for volumetric image compression.

By converting the filter implementation into banded matrix multiplications, lifting [18]–[20] scheme is proposed as another way to implement wavelet transform. Based on it, Srikal *et al.* [21] proposed a neural network-based compression approach with lifting scheme. In [22], the necessity of unitary transform by integer lifting scheme was discussed, and the performance of different integer filter kernels was compared. Rossinelli *et al.* [4] proposed a new lossless data compression scheme based on lifting.

However, all tradition 2-D wavelet transforms above fail to handle 2-D singularities in images [23]. To this end, lines and curves in images are ignored when performing traditional wavelet transform. This problem stems from the fact that 2-D wavelet transform performs 1-D discrete wavelet transform in each direction separately of the 2-D image. To this end, the traditional wavelet transform cannot capture the non-directional features. Moreover, it utilizes these 1-D kernel on the entire image, and cannot capture rich local features such as edges and textures.

2) *Variants of Wavelet Transform* : In order to solve the problems mentioned above, two kinds of variants of traditional wavelet transform have been proposed. One kind of methods include ridgelet transform, curvelet transform and contourlet transform, aiming to solve these problems theoretically. The ridgelet transform [24] was developed to capture straight lines in any directions. The key idea was to convert straight lines into several points by radon transform and then a one-dimension wavelet transform was employed. Curvelet transform [25] was actually a block ridgelet transform to handle curves, which was a more general form compared with ridgelet transform. Contourlet transform [26] had a more flexible multi-resolution, partial, and reverse image expansion. It solved the problems above by performing a directional transform after the subband transform. Note that curvelet and contourlet transforms may produce redundant coefficients, and thus are unsuitable for compression tasks.

The other kind of methods addresses this problem by adaptively selecting filtering directions. Chang *et al.* [27] proposed a direction-adaptive wavelet transform based on direction lifting (ADL). In their method, the local adjustment of the filtering direction was predicted based on image content. Liu *et al.* [28] then proposed a new wavelet transform based on weighted adaptive lifting (WAL), which was an improvement of ADL. It addressed the mismatch between prediction and updating steps.

Although these methods improve the traditional wavelet to a certain extent, there are some unresolved problems at present. First, traditional wavelet transforms are manually designed for ideal signals instead of images. Second, the traditional wavelet basis is fixed when facing different contents. These problems affect the performances of traditional wavelet transforms, which prompt us to find a better solution. Most recently, Ma *et al.* [12], [13] designed a trained wavelet-like reversible transform for end-to-end image compression. Although it is data dependent, it still leads to a fixed wavelet-like basis when facing different contents.

B. Video-based methods

Video-based methods regard a certain dimension of volumetric images as the time dimension. Previous work mostly adjusts the traditional video codec for compressing volumetric images. The bit depth ranges of volumetric images are from 8 to 64. However, video coding codecs often limit the maximum number of coding bits to 16 due to complexity limitations.

To solve this problem, Parikh *et al.* [29] proposed a high bit-depth medical image compression methods using HEVC. Experimental results show that compared with JPEG-2000, using HEVC can improve compression performance by more than 54%. Some other methods aim to improve the lossless compression of HEVC. An improvement to the HEVC intra-frame coding process was proposed in [30] for the lossless compression of gray-scale anatomical medical images, which is characterized by a large number of edges. Guarda *et al.* [31] improved the lossless coding of volumetric medical images for HEVC. Based on Least Squares Prediction (LSP), a new pixel-by-pixel prediction scheme was explored to extend the current HEVC lossless tools.

Although these methods can bring obvious performance improvements, we would still consider that using video-based methods to compress 3-D image is unreasonable. The three dimensions of volumetric images should be treated equal as they are essentially the same. The time dimension should not be distinguished and treated differently.

C. Autoencoder-based methods

Learning-based methods have attracted widespread attention in recent years. Balle *et al.* [32] first proposed an end-to-end fully CNN-based compression method. Then they introduced hyperprior [33] and auto-regressive prior [34] to their methods. Among them, [34] was reported to outperform BPG for the first time. The common part of these popular learning-based methods is that they use an autoencoder as a transform module. However, the autoencoder module is irreversible and causes the loss of information. Some work [8] reported that these popular methods became convergent at high bitrates, and the performance does not increase as the bitrate increases.

Gao *et al.* [6] converted the method mentioned in [34] into its 3-D version to compress brain images. This is also the first time that the learning-based methods are used to compress 3-D images. Because of the use of 3-D autoencoder, their method only surpasses JP3D on very low bitrates. As we know, high-quality reconstruction is essential for volumetric

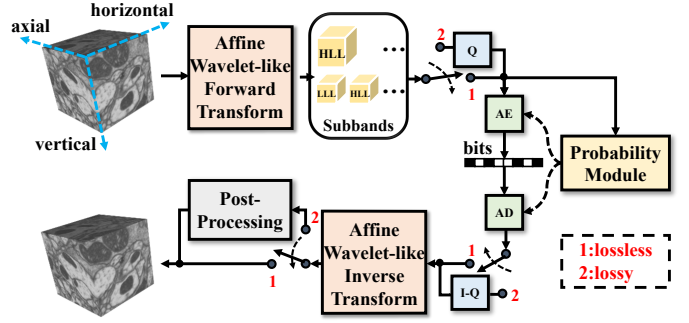


Fig. 1. Overview of our proposed aiWave framework. “Q” and “I-Q” stand for quantization and inverse-quantization module, “AE” and “AD” stand for arithmetic encoding and arithmetic decoding module, respectively. The affine wavelet-like forward transform modules are implemented with 3-D affine lifting operations (see Fig. 2 for the description of 1-D affine lifting operations). The details of two kinds of probability modules we explored are shown in Fig. 5. The post-processing module is utilized to compensate for quantization errors. aiWave can support lossless compression by turning the switch to 1, and lossy compression, turning the switch to 2.

images. Therefore, supporting high-quality reconstruction is a basic requirement for volumetric image compression methods, which is quite different from natural images.

III. PROPOSED FRAMEWORK

In this section, we introduce the proposed versatile volumetric image compression framework aiWave in detail. First, we give an overview of the structure and pipeline of aiWave. Second, we focus on introducing the affine wavelet-like transform module. Third, we discuss the weight sharing strategies of the proposed transform module, followed by the probability and post-processing modules. Finally, we briefly introduce the loss function to train the whole framework.

A. Overview of the framework

Fig. 1 shows our proposed versatile volumetric image compression framework aiWave. It mainly includes four main modules, namely affine wavelet-like forward transform module, probability module, affine wavelet-like inverse transform module, and post-processing module. The overall processes of the encoding and decoding are shown as follows.

In the encoding process, the input image $x \in \mathbb{R}^N$ is converted into a series of subband coefficients y :

$$y = g_a(x; \phi), \quad (1)$$

where $g_a(x; \phi)$ is affine wavelet-like forward transform implemented with 3-D CNNs. Then y is quantized by rounding to its nearest integer:

$$q = [y/QS], \quad (2)$$

where $[\cdot]$ is the rounding operation and QS is the quantization step. It is worth noting that the transform is reversible and does not lead to any loss of information. Only the quantification process introduces loss in the entire framework. Next, the quantized coefficients q are sent to the arithmetic encoder to generate the bit stream. A probability module is used to estimate the probability distribution of coefficients to assist the

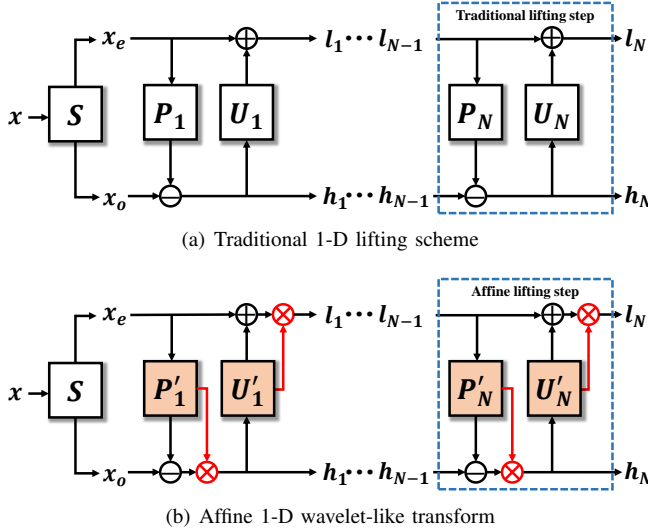


Fig. 2. Difference between 1-D traditional lifting scheme and 1-D affine wavelet-like transform. P_i stands for prediction filter and U_i stands for update filter. P'_i stands for prediction network and U'_i stands for update network. The main difference between the two is that the affine wavelet-like transform additionally predicts an affine map and uses 3D-CNNs to replace the traditional filters. N is the total number of lifting steps in 1-D transform. We use $N=2$ in this paper. For volumetric images, transform is performed three times, first axial-wise, then horizontal-wise and finally vertical-wise.

arithmetic encoder. In this paper, we explore two probability models: a light one implemented by factorized entropy module and a heavy one to further remove redundancy.

In the decoding process, the bit stream is first decoded by an arithmetic decoder with the help of the entropy model. Then, the decoded coefficients are inversely quantized to obtain the coefficient \hat{y} :

$$\hat{y} = q \times QS. \quad (3)$$

Finally, the restored image \hat{x} is obtained by

$$\hat{x} = g_a^{-1}(\hat{y}; \theta). \quad (4)$$

Note that affine wavelet-like inverse transform g_a^{-1} is the inverse of affine wavelet-like forward transform g_a . Finally, \hat{x} is enhanced by the post-processing module to remove compression noise.

When performing lossless compression, the quantization, inverse-quantization, and post-processing modules are removed. At the same time, the transform module should also be changed to its lossless version.

B. Affine wavelet-like transform module

1) **Structure of affine wavelet-like transform:** Our proposed affine wavelet-like transform is built based on traditional lifting scheme. Fig. 2 shows the difference between 1-D traditional lifting scheme and 1-D affine wavelet-like transform.

Traditional lifting scheme includes three operations, namely split, prediction, and update. Through these operations, lifting scheme aims to decompose the original signal into high-frequency and low-frequency components. One prediction operation and one update operation constitute a basic lifting

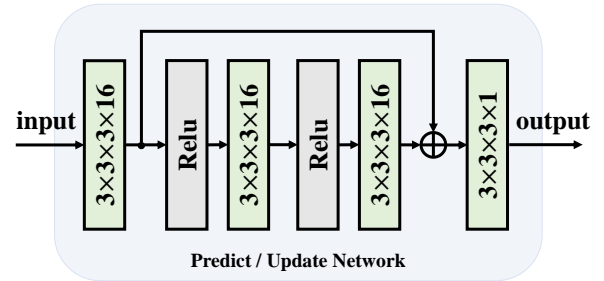


Fig. 3. 3-D convolutional neural network used for each prediction or update step (see Fig. 2). The shown numbers like $3 \times 3 \times 3 \times 16$ indicate the kernel size ($3 \times 3 \times 3$) and the number of output channels (16) of each layer. “Relu” indicates the adopted nonlinear activation function.

step. A split operation incorporating N basic lifting steps forms a 1-D traditional lifting scheme.

We take a 1-D signal as an example to show the detailed lifting scheme. First, the input signal is split into an odd component x_o and an even component x_e ,

$$x_o, x_e = \text{split}(x). \quad (5)$$

Note that there is a strong similarity between x_o and x_e . Therefore, the prediction operation is performed to predict x_o from x_e ,

$$h = x_o - P_i(x_e), \quad (6)$$

where P_i is the prediction filter, and h represents the prediction residual containing high-frequency information of x . Then, h is utilized to update x_e through update operation,

$$l = x_e + U_i(h), \quad (7)$$

where U_i is the update filter, and l contains the coarse details in x , that is, low-frequency information. Note that P_i and U_i in traditional wavelet transform are simple linear filters. For example, in the *CDF 5/3* wavelet, which is used in JP3D for lossless compression, (6) can be written as: $h[m] = x_o[m] - (p_a x_e[m-1] + p_b x_e[m])$, where $p_a = p_b = 0.5$. Different prediction and update filters correspond to different wavelet transforms [19].

Considering that the above prediction and update filters are designed manually, in this paper, we try to replace these filters with 3-D CNNs. The structure of our proposed 3-D CNNs is shown in Fig. 3. In addition, inspired by the generative model glow [35]–[37], we further predict an affine map to adjust the wavelet basis according to the context. Therefore, the proposed affine wavelet-like transform can be written as:

$$x_o, x_e = \text{split}(x), \quad (8)$$

$$h = A(x_e) \odot (x_o - P'_i(x_e)), \quad (9)$$

$$l = B(h) \odot (x_e + U'_i(h)), \quad (10)$$

where P'_i and U'_i represent the prediction and update network, respectively. A and B represent the network for predicting the affine map, which has the same structure with P'_i and U'_i , except that a sigmoid operation is added to limit the values in affine map to the range of 0 to 1. Similar to the traditional lifting scheme, (9) and (10) form a basic affine lifting step. A

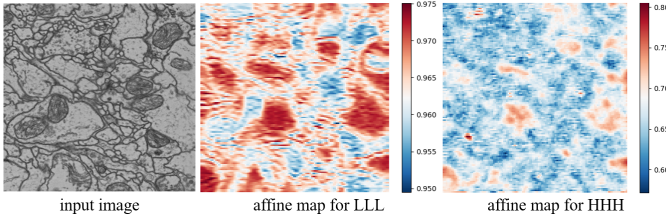


Fig. 4. Visualization results of affine maps. Affine maps for LLL subband and HHH subband are given. It can be seen that the value of the affine map will change as the content of the input image changes. Moreover, the affine value range of different subbands is very different. As shown in this figure, the value of the affine map of the subband LLL is much larger than the value of the affine map of the subband HHH on average.

split operation incorporating N basic affine lifting steps forms a 1-D affine wavelet-like transform.

In the above-mentioned affine wavelet-like transform, the affine map predicts a value for each spatial position. We call it fine-grained affine wavelet-like transform. As shown in Fig. 4, after network training, we find out that the difference between the affine maps is more significant than the different positions of the same affine map. This motivates us to simplify each affine map in the affine wavelet-like transform into a trainable variable, and we call it a coarse-grained affine wavelet-like transform. Results of fine-grained and coarse-grained affine wavelet-like transform are further discussed in Section IV-D.2.

In this work, we first perform 1-D affine wavelet-like transform in the axial direction of the 3-D image. After that, the original signal is decomposed into a low frequency subband L and a high frequency subband H . Then we perform 1-D affine wavelet-like transform on L and H in the horizontal direction, resulting in four subbands $\{LL, HL, LH, HH\}$. For the resulting four subbands, finally, another 1-D affine wavelet-like transform is carried out in the vertical direction, and eight subbands $\{LLL, HLL, LHL, HHL, LLH, HLH, LHH, HHH\}$ are obtained. Three such 1-D affine wavelet-like transforms constitute a complete decomposition. The LLL subband can be further decomposed into eight subbands to make the energy more concentrated. After N times of decomposition, $7N+1$ subbands are obtained. Note that in our method, the parameters of affine wavelet-like transforms in different decomposition levels are shared. To this end, the scale-invariant characteristics of traditional wavelets are still satisfied in our affine wavelet-like transform.

In addition, our affine wavelet-like transform is reversible. The affine wavelet-like inverse transform can be easily obtained from the forward transform as follows:

$$x_e = l/B(h) - U_i'(h), \quad (11)$$

$$x_o = h/A(x_e) + P_i'(x_e), \quad (12)$$

$$x = M(x_e, x_o), \quad (13)$$

where M means the merge operation, which is a reverse operation of split. Note that P_i' , U_i' , A and B network in inverse transform share parameters with that in forward transform.

2) Lossless affine wavelet-like transform: To guarantee lossless compression in a traditional lifting step, a rounding operation is usually added to the prediction and update operations,

$$h = x_o - [P_i'(x_e)], \quad (14)$$

$$l = x_e + [U_i'(h)]. \quad (15)$$

In this way, the entire traditional lifting scheme has only integer operations, thus avoiding loss of precision. However, the situation is different in the proposed affine lifting step. As our method introduces multiplication and division operations, it can bring precision losses especially in hardware implementation.

Some methods [38], [39] have been proposed to address the problem of multiplication and division in reversible networks for lossless compression. In this paper, for simplification, we propose a lossless compression scheme by replacing multiplication and division with left and right shift operations. As we know, bit-wise left or right shift does not bring accuracy loss in hardware implementation. In detail, we first quantize the affine map to the nearest integer power of 2. After that, the multiplication operation is implemented by a right shift operation as the quantized affine map is between 0 and 1,

$$h = RS\{x_o - [P_i'(x_e)], ||\log_2 A(x_e)||\}, \quad (16)$$

$$l = RS\{x_e + [U_i'(h)], ||\log_2 B(h)||\}, \quad (17)$$

where $|\cdot|$ operation means taking the absolute value, and $RS\{h, n\}$ operation stands for shift h to the right by n bits. In the affine wavelet-like inverse transform, the left shift is employed to replace the division operation.

3) Theoretical analysis of affine wavelet-like transform: In this section, we theoretically explain that the proposed affine wavelet-like transform actually improves the wavelet basis of the traditional wavelet transform into a data-driven and content-adaptive form, thus improving performance.

According to [19], the traditional wavelet transform for finite impulse response filter can be decomposed into a lifting scheme by performing factorization. For example, the z-transform of a analysis filter pair (h, g) is denoted by $h(z)$ and $g(z)$, which represent the low-pass and high-pass filter, respectively. Then the corresponding decomposition polyphase matrix $P(z)$ is defined as follows:

$$P(z) = \begin{bmatrix} h_e(z) & h_o(z) \\ g_e(z) & g_o(z) \end{bmatrix} \quad (18)$$

where the $h_e(z)$ and $g_e(z)$ are the even parts and the $h_o(z)$ and $g_o(z)$ are the odd parts of the low-pass and high-pass filter. The polyphase matrix $P(z)$ can be factorized into:

$$P(z) = \prod_{i=1}^m \begin{bmatrix} 1 & s_i(z) \\ 0 & 1 \end{bmatrix} \begin{bmatrix} 1 & 0 \\ t_i(z) & 1 \end{bmatrix} \begin{bmatrix} K & 0 \\ 0 & 1/K \end{bmatrix}, \quad (19)$$

taking the CDF 9/7 filter bank used in JP3D as an example, the CDF 9/7 filter pair can be written as:

$$P(z) = \begin{bmatrix} 1 & \alpha f(z) \\ 0 & 1 \end{bmatrix} \begin{bmatrix} 1 & 0 \\ \beta g(z) & 1 \end{bmatrix} \begin{bmatrix} 1 & \gamma f(z) \\ 0 & 1 \end{bmatrix} \begin{bmatrix} 1 & 0 \\ \delta g(z) & 1 \end{bmatrix} \begin{bmatrix} \zeta & 0 \\ 0 & 1/\zeta \end{bmatrix}, \quad (20)$$

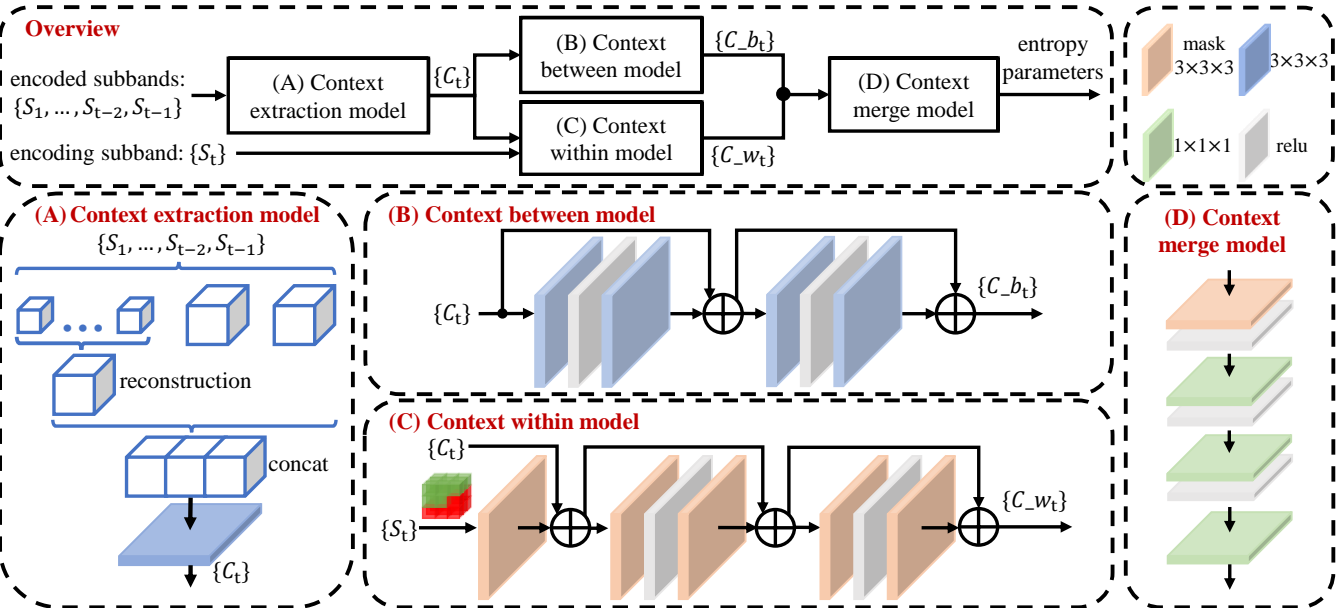


Fig. 5. Structure of context-based entropy module. $3 \times 3 \times 3$ represents the kernel size of CNN and mask $3 \times 3 \times 3$ represents the kernel size of Mask CNN. The main idea of this module is to use the correlation between and within subbands to reduce the uncertainty of the current coded pixels, thereby reducing the bitrate. Firstly, the context extraction model roughly extracts the correlation between subbands (C_t), and C_t is further input into context between model and context within model to extract the context between and within subbands (C_{bt} and C_{wt}). Then context merge model is utilized to fuse these context information and obtains entropy parameters.

where $f(z) = 1 + z^{-1}$, $g(z) = 1 + z$, $\alpha \approx -1.586$, $\beta \approx -0.053$, $\gamma \approx 0.883$, $\delta \approx 0.444$, $\zeta \approx -1.150$. As we know, α , β , γ and δ are the parameters of prediction and update filters in a traditional lifting scheme. ζ is the scaling factor, which can achieve overall scaling for the previous parameters. Therefore, changing these parameters in the lifting scheme actually corresponds to the selection of different wavelet basis in the first generation of wavelets.

In the affine wavelet-like transform, we first replace the prediction and update filters with 3D CNNs. This indicates that we improve the traditional handcrafted wavelet basis to a wavelet-like basis learned from data. More importantly, once the traditional wavelet basis is determined, it does not change when it is used. However, our affine wavelet-like transform additionally predicts an affine map to form the wavelet-like basis, which varies according to different input content. In other words, our affine wavelet-like transform adaptively learns a pixel-wise wavelet basis for each different spatial position similar to a spatial attention mechanism.

C. Weight sharing strategy

It is well known that the physical properties of 2-D natural images in horizontal and vertical directions are exactly the same. Therefore, the traditional wavelet, designed for 2-D images, share parameters in horizontal and vertical directions. However, most 3-D images does not satisfy this property. This phenomenon is caused by the technical limits of the image scanner. Although imaging technologies try to achieve the same resolution in the axial direction (z) as in the lateral direction (x, y), most of them such as serial section transmission EM (ssTEM) fail to collect such thin slices. Thus the image resolution within a slice is much higher

than that between slices in most cases, which means that the correlation in the axial dimension is much smaller than the other two dimensions. Only a few EM, such as focused ion beam scanning EM (FIB-SEM), can collect isotropic data with the same resolution in all three directions through layer by layer corrosion samples.

This inspire us to explore whether the parameter sharing strategy should be adjusted according to the characteristics of the 3-D images. For isotropic data, we propose to share parameters of the prediction and update network in all directions. For anisotropic data, we use a single set of parameters of 3D CNNs to learn wavelets adapted to its characteristics in the axial direction, and share parameters in the other two directions. The detailed experimental results are discussed in Section IV-D.3.

D. Probability module

In this paper, in order to adapt different application scenarios, two kinds of probability modules are employed to estimate the probability distributions of the quantized subband coefficients.

1) **Factorized entropy module:** For scenarios requiring low latency, the factorized entropy module is utilized in our framework and we call this framework aiWave-light.

After transform and quantization, a series of quantized subband coefficients are obtained. The factorized entropy model [33] estimates a continuous probability distribution for each subband. These probabilities can then be used to assist the arithmetic coding process. It is worth mentioning that the subbands are considered as independent and are coded and decoded in parallel in aiWave-light. Therefore, aiWave-light has low coding and decoding complexities and is suitable for scenarios requiring low latency.

TABLE I
DATASETS INTRODUCTION AND TRAINING DETAILS

Name	Category	Species	Position	Characteristic	Bit depth	Training samples	Patch size
FAFB [1]	biological	adult drosophila	brain	anisotropy($4 \times 4 \times 40nm^3$)	8bits	1024	64^3
FIB-25	biological	adult drosophila	brain	isotropy($8 \times 8 \times 8nm^3$)	8bits	1024	64^3
CT [40]	medical	human	spleen	anisotropy(-)	32bits	640	64^3
MRI [41]	medical	human	heart	anisotropy($1.25 \times 1.25 \times 2.7mm^3$)	32bits	983	64^3

2) **Context-based entropy module:** For scenes requiring high performance, we employ a context-based entropy module to further remove redundancies within and between subbands.

As shown in Fig. 5, our context-based entropy module mainly includes four sub-modules. First, the context extraction model is used to roughly obtain the context of the current subband. Then, we employ the context between model and context within model to further extract context information between different subbands and within the same subband through the coded pixels. Finally, a context merge model is employed to fuse these context information and get a series of entropy parameters for probability estimation.

Context extraction model: We employ the context extraction model to roughly extract the context C_t from the encoded subbands $\{S_1, S_2, \dots, S_{t-1}\}$. C_t is further used in context between model and context within model. Note that if the resolution of S_{t-1} is not the same as that of S_t , we synthesize a high-resolution low-frequency subband LLL with the affine wavelet-like inverse transform. After all the coded subbands are integrated, a 3-D convolution is applied to obtain C_t . All the subbands are processed sequentially in a specific order.

Context between model: We employ the context between model to remove redundancies between the current subband and the coded subbands. Multiple 3-D convolutional layers are used to extract high-dimensional features C_{-b_t} from C_t .

Context within model: Motivated by PixelCNN [42], we utilize a context within model to remove redundant information in the same subband. Mask 3-D convolutional layers are used to extract high-dimensional features C_{-w_t} from C_t .

Context merge model: After obtaining the context between subbands and within subbands, we further use a context merge model to fuse them [43]. The network outputs the parameterize cumulative probability distribution through a series of entropy parameters and then differentiate it to obtain the required probability distribution.

E. Post-processing module

As we mentioned above, our transform module is reversible. Therefore, the loss caused by quantization cannot be compensated by the inverse transform. In order to compensate for quantization loss in aiWave, we introduce a post-processing module after affine wavelet-like inverse transform. Specifically, we employ multiple 3-D convolutional layers to construct a 3-D residual block, and the post-processing module contains six 3-D residual blocks. Note that this is quiet different from autoencoder-based frameworks whose decoders can achieve inverse transform and reconstructed image enhancement at the same time.

F. Loss function

During training, we treat the framework as a rate-distortion optimization problem. Thus the loss function becomes:

$$L = R + \lambda \cdot D = \underbrace{\mathbb{E}_{x \sim p_x} [-\log_2 p_q(q)]}_{\text{rate}} + \lambda \cdot \underbrace{\mathbb{E}_{x \sim p_x} \|x - \hat{x}\|_2^2}_{\text{distortion}}, \quad (21)$$

where R and D represents bitrate and distortion, respectively. q stands for quantized coefficients. For each model we specify a Lagrange multiplier λ , which controls the tradeoff between rate and distortion. MSE is utilized to compute the distortion between input image x and reconstruct image \hat{x} .

IV. EXPERIMENTAL RESULTS

A. Datasets and settings

In our experiments, four volumetric image datasets are used for training and testing to demonstrate the effectiveness of the proposed algorithm. Detailed information about theses datasets and the settings of our experiments are shown in Table I. We can see that the bit depths of 3-D CT and MRI dataset are 32. As we know, JP3D and HEVC do not support the volumetric image compression with input bit depth 32. To compare the proposed aiWave with JP3D and HEVC, we scale the CT and MRI images to 16 bits by performing min-max normalization following [44]. Note that different from JP3D and HEVC, our proposed aiWave has no limit on the input bit depth.

We evaluate our aiWave on test data with peak signal-to-noise ratio (PSNR) and compare it with JP3D, HEVC, and autoencoder-based methods. For HEVC, we use the reference software HM-16.15¹ with the random-access configuration. As for JP3D, we use the software OpenJPEG 2.3.1² with the default configuration.

In our training process, we first fix the transform and train the probability and post-processing modules. Then, we fix the probability and post-processing modules and train the affine wavelet-like transform. Finally, we train all modules end-to-end to obtain the final model. The Adam algorithm with its default setting is adopted in the training process. The learning rate is set to $1e^{-4}$. The value of λ in (21) is set to $\{1, 4, 16, 64, 128\}$ to generate bitstream with variable bitrates. The whole training process is carried out on a GTX 1080Ti GPU and takes about 6 days.

B. Performance

1) **Comparison with traditional compression methods:** Fig. 6 shows the rate-distortion (R-D) curve comparison between the

¹<https://vcgit.hhi.fraunhofer.de/jvet/HM/-/tree/HM-16.15>

²<http://www.openjpeg.org/2019/04/02/OpenJPEG-2.3.1-released>

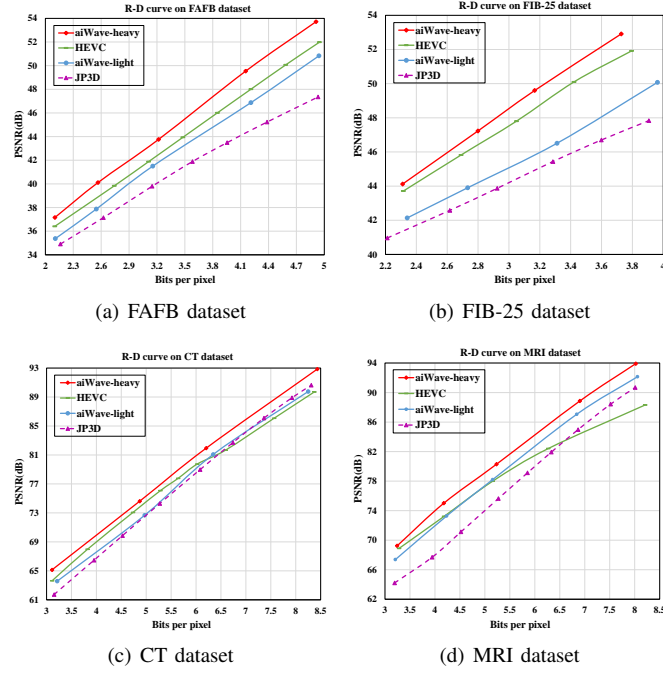


Fig. 6. R-D performance comparisons on FAFB, FIB-25, CT and MRI dataset for lossy compression. "aiWave-heavy" stands for aiWave with context-based entropy module and "aiWave-light" stands for aiWave with factorized entropy module.

proposed aiWave and the traditional compression methods in lossy case, where the rate and distortion are measured by bits per pixel (bpp) and PSNR, respectively. Our aiWave-heavy outperforms all traditional compression methods for all bitrates, and even surpasses HEVC by a large margin. The phenomenon that aiWave-heavy leads to a much better performance than aiWave-light indicates that the context-based entropy module further removes redundancies compared with the factorized entropy module. For the aiWave-light, it outperforms JP3D due to the use of the affine wavelet-like transform and post-processing modules. In order to quantitatively measure the performance, the average Bjontegaard Delta-PSNR (BD-PSNR) improvements of aiWave-heavy compared with the other methods are shown in Fig. 7. Taking the FIB-25 dataset as an example, aiWave-heavy is 0.885dB better than HEVC and 4.206dB better than JP3D on average. In addition, aiWave-light also outperforms JP3D by 0.889dB.

Table II shows the average bits per pixel of various algorithms on the test datasets. It can be seen from the average bpp of aiWave-heavy is the smallest to achieve lossless compression. In addition, aiWave-light performs better than JP3D on all datasets. Among them, the bpp reduction of aiWave on MRI dataset is the most significant. Compared with HEVC and JP3D, the bpps are reduced by 16.2% and 25.5% compared with aiWave-heavy. Meanwhile, aiWave-light also saves 7.5% bits on average compared with JP3D.

2) Comparison with autoencoder-based methods: Fig. 8 shows the comparison between aiWave-heavy and the current state-of-the-art volumetric image compression method based on autoencoder [6]. The experimental results show that Gao *et al.* only achieve a better performance at very low bitrates.

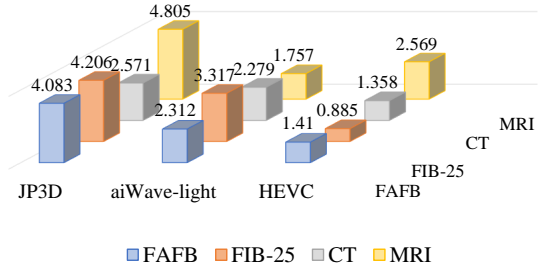


Fig. 7. BD-PSNR improvements of aiWave-heavy compared with the other methods when compared with aiWave-heavy.

TABLE II
AVERAGE BITS PER PIXEL ON FOUR DATASETS FOR LOSSLESS COMPRESSION

Bit Rate	JP3D	HEVC	aiWave-light	aiWave-heavy
FAFB [1]	5.185	6.218	5.122	4.988
FIB-25	5.101	5.170	4.897	4.686
CT [40]	11.890	10.573	11.481	9.833
MRI [41]	11.924	10.605	11.026	8.886

As the bitrate increases, their method converges and the PSNR does not change. This phenomenon is the same as "AE Limit" in 2-D image compression, as claimed in [8]. The autoencoder is irreversible and thus cannot achieve high-quality reconstruction. This experiment further illustrates that our affine wavelet-like transform, a reversible and efficient transform, is more suitable for volumetric image compression.

C. Complexity Analysis

Table III shows the complexities of the proposed framework in terms of encoding/decoding time and the number of parameters. Note that the encoding/decoding time when using GPU is obtained through multi-process parallel acceleration. The 15 subbands obtained after two decompositions are coded and decoded independently in parallel.

It can be seen that the encoding time of aiWave-light is shorter than that of JP3D. This is because our factorized entropy module only relies on the current coefficients when encoding and decoding, and thus can be accelerated in parallel. When decoding, due to the post-processing module, the decoding time of aiWave is slightly slower than JP3D. In other words, our aiWave-light and JP3D have a comparable complexity, but the compression performance of aiWave-light is much better.

Our aiWave-heavy has a slower speed and a larger amount of parameters compared with aiWave-light. This is because each pixel to be encoded depends on all the encoded pixels in context-based entropy module. It trades larger complexity for a significant performance improvement. We also notice that since the decoder does not need to perform RDO, and the code has been optimized and accelerated many times, the decoding speed of HEVC is very fast.

D. Ablation study

1) Comparison of affine wavelet-like transform, additive wavelet-like transform and traditional CDF 9/7 wavelet transform: Fig. 9(a) shows the performance comparisons among

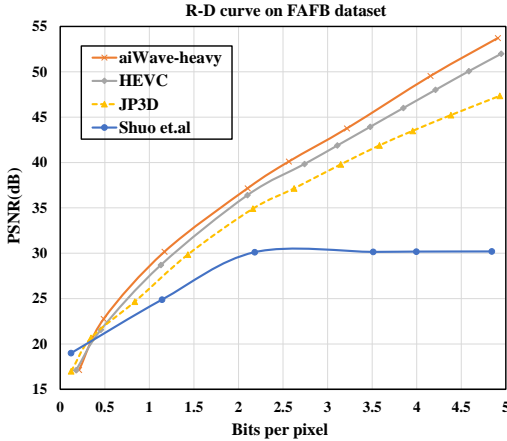


Fig. 8. R-D performance for aiWave-heavy when compared with autoencoder-based method on FAFB dataset.

TABLE III
AVERAGE RUNNING TIME PER IMAGE ON THE FAFB DATASET (IN SECONDS) AND THE NUMBER OF TRAINING PARAMETERS

	JP3D	HEVC	aiWave-light	aiWave-heavy
	CPU	GPU	CPU	GPU
Avg. Enc. Time	0.487	9.617	5.528	0.281
Avg. Dec. Time	0.243	0.052	5.947	0.317
Parameters	-	-	21.3MB	695.5MB

affine wavelet-like transform, additive wavelet-like transform, and traditional CDF 9/7 wavelet transform. The additive wavelet-like transform is obtained through removing the affine map in the affine wavelet-like transform. We can see from Fig. 9(a) that our affine wavelet-like transform significantly outperforms traditional CDF 9/7 wavelet transform by 1.709dB on average. In addition, our affine wavelet-like transform performs better than the additive wavelet-like transform on FAFB dataset, which demonstrates that predicting a context-adaptive affine map indeed brings some performance improvements. Furthermore, the performance of our additive wavelet-like transform is much higher than that of traditional wavelets, which demonstrates that our 3-D learnable wavelet transform significantly improves the performance by replacing traditional manual design through training with a large number of samples.

2) *Comparison of fine-grained and coarse-grained affine wavelet-like transform*: Fig. 9(b) shows the comparison between the fine-grained and coarse-grained affine wavelet-like transforms. As we described in Section III-B, the coarse-grained affine wavelet-like transform is obtained through sharing parameters for all spatial positions. The experimental results show that the coarse-grained affine wavelet-like transform just leads to a little performance degradation. However, the coarse-grained version has a smaller number of parameters, converges faster, and can be trained more stable.

3) *Comparison of different weight sharing strategies for different volumetric images*: Fig. 10 shows the performance of different weight sharing strategies. Anisotropic FAFB dataset and isotropic FIB-25 dataset are applied to represent two kinds of volumetric images.

For an anisotropic dataset, we find that sharing parameters

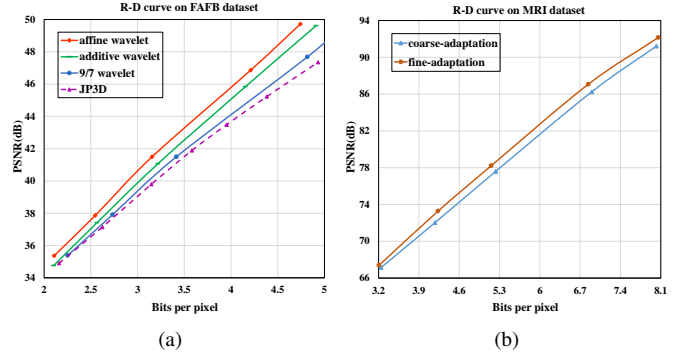


Fig. 9. Subfigure (a) compares the affine wavelet-like transform, the additive wavelet-like transform and the traditional CDF 9/7 wavelet. Subfigure (b) shows the comparison between fine-grained and coarse-grained affine wavelet-like transforms.

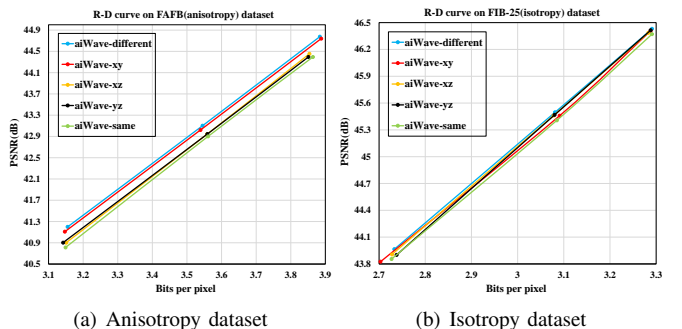


Fig. 10. Comparisons of different parameter sharing strategies. aiWave-different represents that the update and prediction networks in the three directions do not share parameters. aiWave-same shows that all three directions share parameters. aiWave-xy or xz or yz means sharing parameters only in the x and y or x and z or y and z directions.

in the x and y directions while not in the z direction lead to almost the same performance as not sharing parameters in all three directions. Note that using independent parameters in the z direction is about 0.5dB better than using independent parameters in the x or y direction alone even they have the same number of parameters. This phenomenon indicates that the characteristics of the z -direction of anisotropic datasets are different from those of x and y directions. Therefore, we can use independent parameters for the z direction.

For isotropic datasets, we find that even if we do not share parameters in three directions, the performance does not improve significantly compared with sharing parameters in all three directions. This further demonstrates that the isotropic dataset has consistent properties in all three directions. Therefore, all parameters can be shared to reduce complexities without affecting the compression performance.

V. CONCLUSION

In this paper, we propose an end-to-end volumetric image compression framework aiWave, which supports both lossy and lossless compression. We design a trained affine wavelet-like transform to obtain more compact representations of images. Then, we introduce a trainable affine map to enable content-related wavelet-like basis in different spatial regions

of images. After that, we introduce the weight sharing strategies according to the volumetric data characteristics in the axial direction to reduce the number of parameters. Finally, different probability modules are explored to handle different application scenarios. The experimental results demonstrate the superiority of our proposed aiWave compared with the state-of-the-art methods on a variety of 3-D image datasets.

REFERENCES

- [1] Z. Zheng, J. S. Lauritzen, E. Perlman, C. G. Robinson, M. Nichols, D. Milkie, O. Torrens, J. Price, C. B. Fisher, N. Sharifi, *et al.*, “A complete electron microscopy volume of the brain of adult *drosophila melanogaster*,” *Cell*, vol. 174, no. 3, pp. 730–743, 2018.
- [2] S. Wang, S. Tan, Y. Gao, Q. Liu, L. Ying, T. Xiao, Y. Liu, X. Liu, H. Zheng, and D. Liang, “Learning joint-sparse codes for calibration-free parallel MR imaging,” *IEEE transactions on medical imaging*, vol. 37, no. 1, pp. 251–261, 2017.
- [3] L. F. Lucas, N. M. Rodrigues, L. A. da Silva Cruz, and S. M. de Faria, “Lossless compression of medical images using 3-D predictors,” *IEEE transactions on medical imaging*, vol. 36, no. 11, pp. 2250–2260, 2017.
- [4] D. Rossinelli, G. Fourestey, F. Schmidt, B. Busse, and V. Kurtcuoglu, “High-throughput lossy-to-lossless 3D image compression,” *IEEE Transactions on Medical Imaging*, 2020.
- [5] M. Hernández-Cabronero, V. Sanchez, I. Blanes, F. Auli-Llinas, M. W. Marcellin, and J. Serra-Sagristà, “Mosaic-based color-transform optimization for lossy and lossy-to-lossless compression of pathology whole-slide images,” *IEEE transactions on medical imaging*, vol. 38, no. 1, pp. 21–32, 2018.
- [6] S. Gao, Y. Zhang, D. Liu, and Z. Xiong, “Volumetric end-to-end optimized compression for brain images,” in *2020 IEEE International Conference on Visual Communications and Image Processing (VCIP)*, pp. 503–506, IEEE, 2020.
- [7] S. Gao and Z. Xiong, “Deep enhancement for 3D HDR brain image compression,” in *2019 IEEE International Conference on Image Processing (ICIP)*, pp. 714–718, IEEE, 2019.
- [8] L. Helminger, A. Djelouah, M. Gross, and C. Schroers, “Lossy Image Compression with Normalizing Flows,” *arXiv preprint arXiv:2008.10486*, 2020.
- [9] S. Bhavani and K. Thanushkodi, “A survey on coding algorithms in medical image compression,” *International Journal on Computer Science and Engineering*, vol. 2, no. 5, pp. 1429–1434, 2010.
- [10] P. Kumar and A. Parmar, “Versatile approaches for medical image compression: a review,” *Procedia Computer Science*, vol. 167, pp. 1380–1389, 2020.
- [11] T. Bruylants, P. Schelkens, and A. Tzannes, “JP3D-Extensions for Three-Dimensional Data (Part 10),” in *The JPEG 2000 Suite*, pp. 199–227, Wiley-Blackwell, 2009.
- [12] H. Ma, D. Liu, R. Xiong, and F. Wu, “iWave: CNN-Based Wavelet-Like Transform for Image Compression,” *IEEE Transactions on Multimedia*, vol. 22, no. 7, pp. 1667–1679, 2019.
- [13] H. Ma, D. Liu, N. Yan, H. Li, and F. Wu, “End-to-End Optimized Versatile Image Compression With Wavelet-Like Transform,” *IEEE Transactions on Pattern Analysis and Machine Intelligence*, 2020.
- [14] D. Xue, H. Ma, L. Li, D. Liu, and Z. Xiong, “iWave3D: End-to-end brain image compression with trainable 3-D wavelet transform,” 2021.
- [15] D. Ravichandran, M. G. Ahamad, and M. A. Dhivakar, “Performance analysis of three-dimensional medical image compression based on discrete wavelet transform,” in *2016 22nd International Conference on Virtual System & Multimedia (VSMM)*, pp. 1–8, IEEE, 2016.
- [16] J. Wang and K. Huang, “Medical image compression by using three-dimensional wavelet transformation,” *IEEE Transactions on Medical Imaging*, vol. 15, no. 4, pp. 547–554, 1996.
- [17] G. U. V. Selvi and R. Nadarajan, “CT and MRI image compression using wavelet-based contourlet transform and binary array technique,” *Journal of Real-Time Image Processing*, vol. 13, no. 2, pp. 261–272, 2017.
- [18] W. Sweldens, “The lifting scheme: A construction of second generation wavelets,” *SIAM journal on mathematical analysis*, vol. 29, no. 2, pp. 511–546, 1998.
- [19] I. Daubechies and W. Sweldens, “Factoring wavelet transforms into lifting steps,” *Journal of Fourier analysis and applications*, vol. 4, no. 3, pp. 247–269, 1998.
- [20] W. Sweldens, “The lifting scheme: A custom-design construction of biorthogonal wavelets,” *Applied and computational harmonic analysis*, vol. 3, no. 2, pp. 186–200, 1996.
- [21] P. Srikala and S. Umar, “Neural network based image compression with lifting scheme and RLC,” *International Journal of Research in Engineering and Technology*, vol. 1, no. 1, pp. 13–19, 2012.
- [22] G. Ginesu, D. D. Giusto, and W. A. Pearlman, “Lossy to lossless SPIHT-based volumetric image compression,” in *2004 IEEE International Conference on Acoustics, Speech, and Signal Processing*, vol. 3, pp. iii–693, IEEE, 2004.
- [23] T. Bruylants, A. Munteanu, and P. Schelkens, “Wavelet based volumetric medical image compression,” *Signal processing: Image communication*, vol. 31, pp. 112–133, 2015.
- [24] M. N. Do and M. Vetterli, “The finite ridgelet transform for image representation,” *IEEE Transactions on image Processing*, vol. 12, no. 1, pp. 16–28, 2003.
- [25] J. Ma and G. Plonka, “The curvelet transform,” *IEEE signal processing magazine*, vol. 27, no. 2, pp. 118–133, 2010.
- [26] M. N. Do and M. Vetterli, “The contourlet transform: an efficient directional multiresolution image representation,” *IEEE Transactions on image processing*, vol. 14, no. 12, pp. 2091–2106, 2005.
- [27] C.-L. Chang and B. Girod, “Direction-adaptive discrete wavelet transform for image compression,” *IEEE Transactions on Image Processing*, vol. 16, no. 5, pp. 1289–1302, 2007.
- [28] Y. Liu and K. N. Ngan, “Weighted adaptive lifting-based wavelet transform for image coding,” *IEEE Transactions on Image Processing*, vol. 17, no. 4, pp. 500–511, 2008.
- [29] S. S. Parikh, D. Ruiz, H. Kalva, G. Fernández-Escribano, and V. Adzic, “High-bit-depth medical image compression with HEVC,” *IEEE journal of biomedical and health informatics*, vol. 22, no. 2, pp. 552–560, 2017.
- [30] V. Sanchez and J. Bartrina-Rapesta, “Lossless compression of medical images based on HEVC intra coding,” in *2014 IEEE International Conference on Acoustics, Speech and Signal Processing (ICASSP)*, pp. 6622–6626, IEEE, 2014.
- [31] A. F. Guarda, J. M. Santos, L. A. da Silva Cruz, P. A. Assuncao, N. M. Rodrigues, and S. M. de Faria, “A method to improve HEVC lossless coding of volumetric medical images,” *Signal Processing: Image Communication*, vol. 59, pp. 96–104, 2017.
- [32] J. Ballé, V. Laparra, and E. P. Simoncelli, “End-to-end optimized image compression,” *arXiv preprint arXiv:1611.01704*, 2016.
- [33] J. Ballé, D. Minnen, S. Singh, S. J. Hwang, and N. Johnston, “Variational image compression with a scale hyperprior,” *arXiv preprint arXiv:1802.01436*, 2018.
- [34] D. Minnen, J. Ballé, and G. Toderici, “Joint autoregressive and hierarchical priors for learned image compression,” *arXiv preprint arXiv:1809.02736*, 2018.
- [35] L. Dinh, D. Krueger, and Y. Bengio, “Nice: Non-linear independent components estimation,” *arXiv preprint arXiv:1410.8516*, 2014.
- [36] L. Dinh, J. Sohl-Dickstein, and S. Bengio, “Density estimation using real nvp,” *arXiv preprint arXiv:1605.08803*, 2016.
- [37] D. P. Kingma and P. Dhariwal, “Glow: Generative flow with invertible 1x1 convolutions,” *arXiv preprint arXiv:1807.03039*, 2018.
- [38] E. Hoogeboom, J. W. Peters, R. v. d. Berg, and M. Welling, “Integer discrete flows and lossless compression,” *arXiv preprint arXiv:1905.07376*, 2019.
- [39] S. Zhang, C. Zhang, N. Kang, and Z. Li, “iVPF: Numerical invertible volume preserving flow for efficient lossless compression,” in *Proceedings of the IEEE/CVF Conference on Computer Vision and Pattern Recognition*, pp. 620–629, 2021.
- [40] A. L. Simpson, J. N. Neal, A. Pugalethi, P. J. Allen, R. P. DeMatteo, Y. Fong, M. Gönen, W. R. Jarnagin, T. P. Kingham, M. I. Miga, *et al.*, “Chemotherapy-induced splenic volume increase is independently associated with major complications after hepatic resection for metastatic colorectal cancer,” *Journal of the American College of Surgeons*, vol. 220, no. 3, pp. 271–280, 2015.
- [41] C. Tobon-Gomez, A. J. Geers, J. Peters, J. Weese, K. Pinto, R. Karim, M. Ammar, A. Daoudi, J. Margeta, Z. Sandoval, *et al.*, “Benchmark for algorithms segmenting the left atrium from 3D CT and MRI datasets,” *IEEE transactions on medical imaging*, vol. 34, no. 7, pp. 1460–1473, 2015.
- [42] A. v. d. Oord, N. Kalchbrenner, O. Vinyals, L. Espeholt, A. Graves, and K. Kavukcuoglu, “Conditional image generation with PixelCNN decoders,” *arXiv preprint arXiv:1606.05328*, 2016.
- [43] F. Mentzer, E. Agustsson, M. Tschannen, R. Timofte, and L. Van Gool, “Conditional probability models for deep image compression,” in *Proceedings of the IEEE Conference on Computer Vision and Pattern Recognition*, pp. 4394–4402, 2018.

[44] F. Wang, R. Jiang, L. Zheng, C. Meng, and B. Biswal, “3D U-net based brain tumor segmentation and survival days prediction,” in *International MICCAI Brainlesion Workshop*, pp. 131–141, Springer, 2019.